Development 138, 4685-4697 (2011) doi:10.1242/dev.068031

COUP-TFI promotes radial migration and proper morphology of callosal projection neurons by repressing Rnd2 expression

Christian Alfano[1,2,3], Luigi Viola[1], Julian Ik-Tsen Heng[4,*], Marinella Pirozzi[1], Michael Clarkson[2,3], Gemma Flore[1], Antonia De Maio[1], Andreas Schedl[2,3], François Guillemot[4] and Michèle Studer[1,2,3,†]

SUMMARY

During corticogenesis, late-born callosal projection neurons (CPNs) acquire their laminar position through glia-guided radial migration and then undergo final differentiation. However, the mechanisms controlling radial migration and final morphology of CPNs are poorly defined. Here, we show that in COUP-TFI mutant mice CPNs are correctly specified, but are delayed in reaching the cortical plate and have morphological defects during migration. Interestingly, we observed that the rate of neuronal migration to the cortical plate normally follows a low-rostral to high-caudal gradient, similar to that described for COUP-TFI. This gradient is strongly impaired in *COUP-TFI*$^{-/-}$ brains. Moreover, the expression of the Rho-GTPase *Rnd2*, a modulator of radial migration, is complementary to both these gradients and strongly increases in the absence of COUP-TFI function. We show that COUP-TFI directly represses *Rnd2* expression at the post-mitotic level along the rostrocaudal axis of the neocortex. Restoring correct *Rnd2* levels in *COUP-TFI*$^{-/-}$ brains cell-autonomously rescues neuron radial migration and morphological transitions. We also observed impairments in axonal elongation and dendritic arborization of *COUP-TFI*-deficient CPNs, which were rescued by lowering *Rnd2* expression levels. Thus, our data demonstrate that COUP-TFI modulates late-born neuron migration and favours proper differentiation of CPNs by finely regulating *Rnd2* expression levels.

KEY WORDS: Radial migration, Cerebral cortex, Callosal projection neurons, Dendrite morphology, COUP-TFI, Rnd2, Mouse

INTRODUCTION

The mammalian neocortex has undergone pronounced expansion in size and complexity during evolution and is responsible for high cognitive function, sensory perception and consciousness (Northcutt and Kaas, 1995). Newborn neurons migrate from the ventricular zone (VZ) to the pial surface and settle in the cortical plate (CP) in a sequential manner with deeper layers (DLs) formed first, followed by upper layers (ULs) (Rakic, 1978; Super and Uylings, 2001). The latter are developmentally and phylogenetically the last structure to appear in the mammalian cortex (Aboitiz et al., 2003; Molnar et al., 2006). Novel specialized neuronal subpopulations with a high degree of complexity of dendritic and axonal arborization have evolved in the uppermost layers. Callosal projection neurons (CPNs), for example, represent a heterogeneous population of UL pyramidal neurons prevalently located in layers II and III of the neocortex (Molyneaux et al., 2009; Ramos et al., 2008) and projecting either ipsilaterally or to homotypic regions of the contralateral hemisphere, giving rise to the corpus callosum (CC) (Mitchell and Macklis, 2005; Richards et al., 2004).

It has been hypothesized that the inside-out pattern of corticogenesis leading to the birth of the six-layered neocortex was made possible by the appearance of glia-guided neuronal migration (Aboitiz et al., 2003; Molnar et al., 2006). Early-born neurons give rise to layers VI and V (phylogenetically older structures), essentially by somal translocation (Miyata et al., 2004; Nadarajah et al., 2002), whereas late-born neurons follow a complex pattern of migration. During early phases, late-born neurons adopt a multipolar morphology and migrate through the subventricular zone (SVZ) independently of the radial glia scaffold (LoTurco and Bai, 2006; Tabata and Nakajima, 2003). In the upper intermediate zone (IZ), migrating neurons assume a bipolar shape, attach to radial glia and move to the CP by glia-guided locomotion (LoTurco and Bai, 2006; Tabata and Nakajima, 2003). Finally, during late phases of the migratory process, bipolar neurons contact the pial surface detaching from the glia scaffold and reach their target by somal translocation, thus allowing glia-guided upcoming neurons to reach upper positions (Nadarajah et al., 2001).

In the last 20 years, many molecules have been reported to be required for different steps of this process. For example, Lis1 (Pafah1b1 – Mouse Genome Informatics), Dcx, FlnA (LoTurco and Bai, 2006), Cdk5 (Ohshima et al., 2007) and RhoA (Ge et al., 2006; Hand et al., 2005) control multipolar-shaped cell (MSC) migration and the transition from MSCs to bipolar-shaped cells (BSCs) in the IZ. Other molecules, like Mdga1 (Takeuchi and O'Leary, 2006), N-cofilin (Bellenchi et al., 2007), α3β1 and α5β1 integrins (Dulabon et al., 2000; Marchetti et al., 2010) and Dcx are implicated in the maintenance of bipolar cell polarity and interaction of migrating neurons with the radial glia. Finally, the secreted molecule Reelin and its downstream effector Dab1 guide the detachment of migrating neurons from the radial glia, allowing the final somal translocation step beneath the pial surface (Dulabon et al., 2000; Olson et al., 2006; Sanada et al., 2004). Remarkably, disruption of many of these molecules not only leads to impairment in radial migration and lamination, but also causes a striking alteration in dendritic and axonal morphology of UL neurons. However, the correlation between cell shape transition from MSC to BSC and the final morphology and connectivity of UL neurons is still elusive.

[1]Telethon Institute of Genetics and Medicine (TIGEM), Developmental Disorders Program, 80131 Naples, Italy. [2]INSERM, U636, Nice, F-06108, France. [3]University of Nice Sophia-Antipolis, U636, F-06108, France. [4]Department of Molecular Neurobiology, National Institute of Medical Research, London NW7 1AA, UK.

*Present address: The Australian Regenerative Medicine Institute, c/o Monash University, Clayton VIC 3800, Australia
[†]Author for correspondence (michele.studer@unice.fr)

Accepted 16 August 2011

Although the number of molecules found to be involved in the regulation of glia-guided radial migration has increased remarkably in recent years, very little is known about their transcriptional regulation. The proneural gene Ngn2 (Neurog2 – Mouse Genome Informatics) was the first factor discovered to activate directly the expression of one of these factors, the small Rho-GTPase Rnd2, which is involved in the regulation of MSC-to-BSC transition and BSC migration during mid-late stages of corticogenesis (Heng et al., 2008; Nakamura et al., 2006). Although Rnd2 transcription is activated by Ngn2 primarily in MSCs along the SVZ and the lower IZ (Heng et al., 2008; Nakamura et al., 2006), its expression was also shown to be enhanced by NeuroD2, a transcription factor that is strongly expressed in the IZ and CP during mid-late stages of corticogenesis (Heng et al., 2008). However, Rnd2 expression is sharply downregulated in the upper IZ, where BSCs attach to the glia and migrate to the CP, suggesting that an independent pathway might negatively regulate Rnd2 expression in this compartment and that such a step might be relevant for correct BSC migration to the CP.

In this study, we found that in the absence of COUP-TFI (Nr2f1 – Mouse Genome Informatics), a transcription factor crucial for corticogenesis and arealization (Armentano et al., 2006; Armentano et al., 2007; Tomassy et al., 2010), Rnd2 expression is abnormally high in the SVZ and IZ during glia-guided radial migration. As a consequence, a greater number of MSCs are stalled in the IZ and BSC migration to the CP is impaired. Although normally specified, CPNs show defects in their postnatal dendritic morphology and in the elongation and arborization of their axons. Unexpectedly, lowering *Rnd2* levels in COUP-TFI-deficient neurons rescues migratory defects of *COUP-TFI*$^{-/-}$ CPNs, which remarkably recover their morphology in a cell-autonomous manner. In conclusion, we demonstrate that Rnd2 expression levels are precisely fine-tuned by COUP-TFI and are essential for CPN radial migration and maturation.

MATERIALS AND METHODS

Animals

COUP-TFI null (*COUP-TFI*$^{-/-}$) and *COUP-TFI fl/fl* mice were generated and genotyped as previously shown (Armentano et al., 2006; Armentano et al., 2007). *COUP-TFI fl/fl* mice were either crossed to *Emx1-Cre* for inactivating COUP-TFI in progenitors (*COUP-TFI CKO-Emx1*) (Armentano et al., 2007) or to *Nex-Cre* for COUP-TFI inactivation in post-mitotic cells (Goebbels et al., 2006). *COUP-TFI*$^{-/-}$ were crossed to the *Ngn2*^{KIGFP} mouse line (Seibt et al., 2003) to generate double mutants, *COUP-TFI/Ngn2 dKO*. Midday of the day of the vaginal plug was embryonic day (E) 0.5. All experiments were conducted following guidelines of the Institutional Animal Care and Use Committee, Cardarelli Hospital, Naples, Italy.

BrdU birthdating

Timed pregnant females received a single intraperitoneal injection of 5-bromo-2′-deoxyuridine (BrdU; 50 mg/kg) at 14.5 days post-coitum (dpc) and three wild-type (wt) and three *COUP-TFI*$^{-/-}$ embryos were collected at E16.5. Five regions (three sections per region) were arbitrarily chosen along the rostrocaudal axis and BrdU+ cells were counted with the NIH ImageJ software in a 250 μm-wide portion of the IZ and the CP compartments of the lateral cortex. The number of CP BrdU+ cells was expressed as a percentage of total CP/IZ BrdU+ cells.

Immunofluorescence, immunohistochemistry and in situ hybridization

Vibratome and cryostat sections were processed for immunocytochemistry and/or in situ hybridization as previously described (Armentano et al., 2007). The following primary antibodies were used: rabbit anti-GFP antibody (1:1000, Chemicon); goat anti-Cux1 (1:50, Santa Cruz); mouse anti-BrdU (1:300, Sigma); rabbit anti-activated caspase 3 (1:100, Cell Signaling Technology); mouse anti-human COUP-TFI (1:100, Abcam); rabbit anti-COUP-TFI (1:500) (Tripodi et al., 2004); rat anti-CTIP2 (1:500, Abcam); mouse anti-Nestin (1:100, Chemicon); rabbit anti-Pax6 (1:100, Chemicon); mouse anti-Satb2 (1:20, Abcam); rabbit anti-Tbr1 (1:1000, gift from R. Hevner, University of Washington, Seattle, USA) and rabbit anti-Cre (1:100, Covance). The following secondary antibodies were used: Alexa Fluor 488-conjugated anti-rabbit; Alexa Fluor 594-conjugated anti-rabbit; Alexa Fluor 594-conjugated anti-mouse; Alexa Fluor 488-conjugated anti-mouse (1:400, Molecular Probes). Antisense RNA Probes were labelled using a DIG-RNA Labelling Kit (Roche).

In utero and ex vivo electroporation and organotypic slice cultures

The *pCIG2-IRES-GFP*, *pCIG2-Cre-IRES-GFP*, *Rnd2*-specific (*SH1*, *SH2*) and scrambled (*SCR*) *shRNA-IRES-GFP* (Heng et al., 2008) plasmids were injected into E14.5 embryonic vesicles with a PV820 Pneumatic PicoPump (WPI). The electroporations were performed on whole heads using a Tweezertrode electrode (diameter 7 mm; BTX) connected to a CUY 21 EDIT electroporator (NEPA GENE) with the following parameters: five 50 V pulses, P(on) 50 mseconds, P(off) 1 second. Brains were then embedded in 3% agarose and cut using a vibratome (Leica VT1000S) at 300 μm thickness. Slices were cultured for 4 days in Neurobasal Medium (GIBCO) plus N12 and B27 supplements (GIBCO), as previously described (Tripodi et al., 2004). In utero electroporations were performed as previously described (Nguyen et al., 2006) with the following parameters: four 40 V pulses, P(on) 50 mseconds, P(off) 1 second. Analysis of GFP+ cell distribution was performed on the lateral cortex along the rostrocaudal axis. The cortex was subdivided into VZ/SVZ, IZ and CP compartments, and the IZ and CP were further subdivided in lower, medial and upper subcompartments (Heng et al., 2008; Nguyen et al., 2006). Cell counts in the different subcompartments were performed on at least three 10 μm thick planes scanned at different depths of each single slide. The number of GFP+ cells for each compartment was expressed as a percentage of the total number of GFP+ cells. The mean value of GFP+ cells counted in each compartment of the three planes was used to calculate the average value among the same neocortical compartments of rostrocaudal slices from at least three littermates for each genotype.

Real-time PCR analysis

The neocortex of three wt and three *COUP-TFI*$^{-/-}$ brains was dissected and immediately transferred to 500 μl of Trizol (Invitrogen) and processed for total RNA isolation according to the manufacturer's protocol. RNA (1 μg) was reverse transcribed using a QuantiTect Reverse Transcription Kit (Qiagen). Real-time PCR (QPCR) analysis was performed for all the littermates in triplicate on a 7900HT Fast Real Time PCR System (Applied Biosystems). The PCR reaction was performed using Power SYBR Green PCR Master Mix (Applied Biosystems) according to the manufacturer's protocol. All the assays were normalized with respect to Gapdh values. Fold-change variations in the levels of mRNA of interest were expressed as a percentage and normalized against wt levels (set as 100%). For primers see Table S2 in the supplementary material.

Chromatin immunoprecipitation (ChIP)

For each experiment (n=3), neocortices were dissected from 24 mice at E14.5 and diced in ice cold Hanks Buffered Saline Solution (GIBCO). Nuclei were processed and ChIP was performed as described in Kuo and Allis, 1999 (Kuo and Allis, 1999). Antisera directed against COUP-TFI (15 μl) or 3 μg Dicer (Santa Cruz sc30226 as Rabbit IgG control) were used for immunoprecipitation. Putative COUP-TFI binding sites were tested by QPCR analysis of ChIP samples using the LightCycler 480 Real-Time PCR System (Roche). Reactions were performed in triplicate on three independently prepared ChIP samples. Amplification was expressed as fold enrichment compared with non-specific IgG control and relative quantities of immunoprecipitated DNA were calculated as previously described (Heng et al., 2008). For primers see Table S2 in the supplementary material.

Statistical analysis

All the data were statistically analyzed and graphically represented using Microsoft Office Excel software. The error bars represent s.e.m. Two-tailed Student's t-test was used for the analysis of statistical significance (*$P \leq 0.05$,

**$P \leq 0.01$, ***$P \leq 0.005$). One-way analysis of variance (ANOVA) was used to compare the means among three or more groups of samples and post-hoc analysis was performed by two-tailed Student's *t*-test.

Image acquisition

Images were acquired with an Upright microscope Leica DM5000B equipped with Leica IM image management software (Leica Microsystems, Wetzlar, Germany). A Zeiss LSM 710 Laser Scanning Microscope (Carl Zeiss MicroImaging, Jena, Germany) and a Fluorescence Inverted Confocal Microscope LEICA SP2 AOBS (Leica Microsystems, Heidelberg, Germany) were used for image acquisition of ex vivo and in utero electroporated brain slices. A total of 23 *z*-line scans with a step distance of 0.45 µm were collected at different depths along the *z*-axis of each lateral neocortex (one to four different regions along the *z*-axis were scanned depending on the thickness of the electroporated area) and maximum intensity projections were generated either using Zeiss ZEN Confocal Software (Carl Zeiss MicroImaging) or using Leica Confocal Software (Leica Microsystems, Wetzlar, Germany).

Cell transfection, protein extraction and western blotting

The mouse embryocarcinoma cell line P19 was transfected at 60% confluence with *pCIG2-[Flag-Rnd2]-IRES-GFP* and *shRNA-IRES-GFP* vectors (Heng et al., 2008) using Lipofectamine 2000 Transfection Reagent (Invitrogen) according to the manufacturer's protocol. Total protein extraction and western blotting were performed as previously described (Armentano et al., 2006). The following primary antibodies were used: mouse monoclonal anti-Flag (1:1000, Sigma), mouse anti-β3 tubulin (1:1000, Sigma); and appropriate secondary antibodies: goat anti-mouse IgG (H+L) horseradish peroxidase conjugate (1:5000, Bio-Rad). The signal was detected with ECL reagent (Amersham Biosciences).

Morphological analysis of the corpus callosum

Brains of three wt and five *COUP-TFI CKO-Emx1* P60 mice were vibratome-sectioned coronally at a thickness of 50 µm and processed for Nissl staining, as previously described (Tomassy et al., 2010). Pictures were taken on a LEICA MZ 16 FA Stereomicroscope and converted from RGB to BW by Adobe Photoshop software. Section images were identified with serial numbers and analyzed in both hemispheres, spanning the entire tract. Using a graphic pen, all the different callosal components were labelled with different colours, and images were aligned and integrated by Amira 4.1.2-1 software to obtain 3D pictures.

RESULTS

Newborn UL neurons are properly specified but abnormally positioned in *COUP-TFI*$^{-/-}$ mice

To investigate the mechanisms underlying alteration of ULs in the absence of COUP-TFI function (Armentano et al., 2007; Faedo et al., 2008; Tomassy et al., 2010), we first assessed whether late-born neurons were normally specified in *COUP-TFI*$^{-/-}$ mice. The expression of Satb2, required for late specification of CPNs (Alcamo et al., 2008; Britanova et al., 2008), as well as the expression of Cux1 and Cux2, involved in early and late differentiation of late-born neurons (Cubelos et al., 2010; Nieto et al., 2004; Zimmer et al., 2004), were affected in mutant ULs at P0 (Fig. 1A). The dense

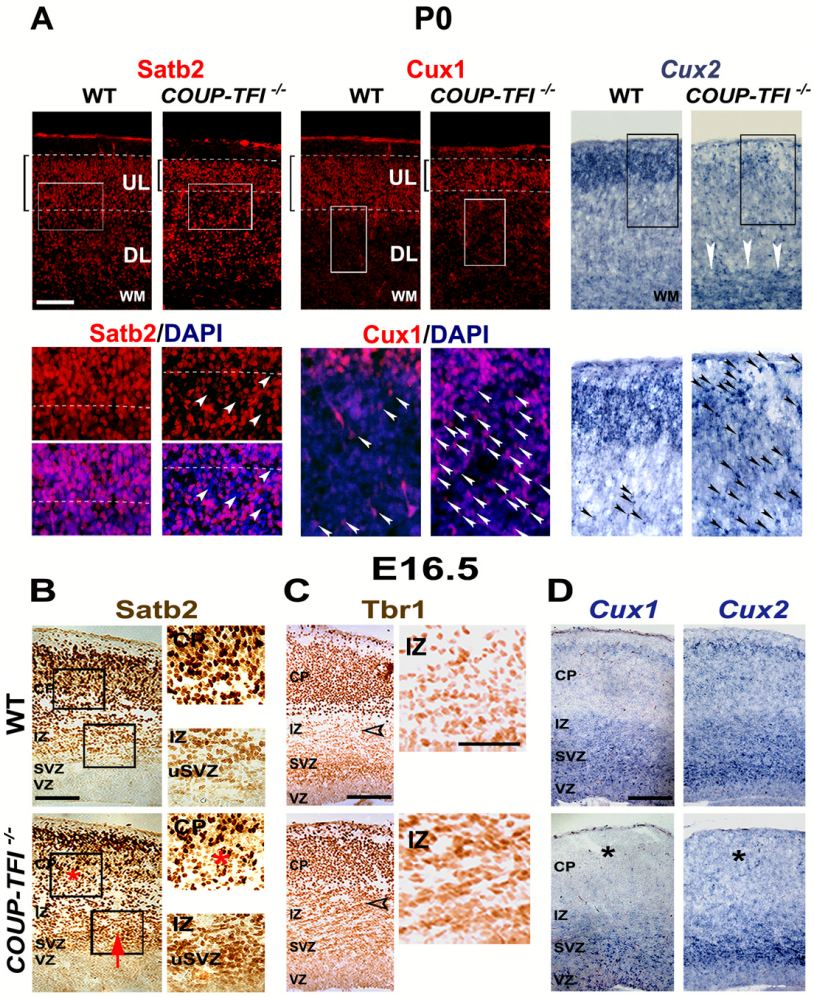

Fig. 1. Abnormal distribution of differentiation markers in *COUP-TFI*$^{-/-}$ mouse neocortices. (**A**) Immunostaining for Satb2 and Cux1 of P0 coronal sections reveals decreased thickness (dashed lines and brackets) of upper layers (UL) in COUP-TFI mutant (*COUP-TFI*$^{-/-}$) brains. *Cux2* expression is strongly impaired in mutant ULs whereas it remains high in the white matter (WM; arrowheads). Many neurons fail to express Satb2 in upper regions of the cortex (arrowheads in square panels), whereas scattered Cux1- and *Cux2*-positive cells are abnormally positioned in deep layers (DL) of mutant brains (lower panels and arrowheads). Lower panels are magnifications of the boxed areas in the respective upper panels. (**B**) Satb2 expression is increased in the SVZ/IZ of *COUP-TFI*$^{-/-}$ E16.5 medial coronal sections (arrow), whereas its expression is decreased in the mutant CP (asterisk). Right-hand panels are magnifications of the boxed areas in the respective left-hand panels. (**C**) Tbr1 expression increases in the IZ of *COUP-TFI*$^{-/-}$ E16.5 coronal sections (arrowheads). (**D**) *Cux1* and *Cux2* expression is undetectable in the CP of *COUP-TFI*$^{-/-}$ E16.5 coronal sections (asterisks). Scale bars: 200 µm for A-D except C, square panel (100 µm). uSVZ, upper SVZ.

Satb2- and Cux1-positive upper cell layer was reduced in thickness and scattered Cux1- and *Cux2*-positive cells were observed along the radial extent of the mutant cortex. At E16.5, when late-born neurons are predominantly migrating, increased expression of Satb2 and Tbr1, a marker of post-mitotic projection neurons (Hevner et al., 2001) was observed in the upper SVZ and IZ of mutant brains (Fig. 1B,C). No double positive cells for Satb2 and Tbr2 (Eomes – Mouse Genome Informatics), an intermediate progenitor marker (Englund et al., 2005; Kowalczyk et al., 2009; Sessa et al., 2008) were found in *COUP-TFI*$^{-/-}$ brains, similarly to control brains (see Fig. S1A in the supplementary material), excluding precocious expression of Satb2 in early post-mitotic neurons. In addition, Satb2 expression was decreased in the CP and *Cux1* and *Cux2* showed weak or absent expression in the CP (asterisks in Fig. 1D), suggesting overall abnormal cell migration rather than abnormal specification of late-born neurons in the absence of COUP-TFI function.

Loss of COUP-TFI affects neuronal radial migration in presumptive somatosensory cortex

To investigate further whether absence of COUP-TFI has an effect on radial cell migration during mid-late corticogenesis, we injected BrdU into pregnant females at 14.5 dpc and evaluated the percentage of BrdU+ cells in the CP of E16.5 wt and *COUP-TFI*$^{-/-}$ brains along their rostrocaudal axis (Fig. 2A,B; see Table S1 in the supplementary material). The number of BrdU+ cells in the CP was expressed as a percentage of the BrdU+ cells in the IZ/CP regions (Fig. 2B) to avoid any interference derived from increased proliferation of mutant progenitor cells in the VZ/SVZ (Faedo et al., 2008). Interestingly, we observed a significantly lower percentage of cells reaching the CP in mediolateral regions of mutant neocortices (presumptive somatosensory area), whereas rostral- and caudal-most regions were unaffected (Fig. 2B; see Table S1 in the supplementary material).

Next, we assessed directly the behaviour of abnormally migrating cells by ex vivo electroporation (Hand et al., 2005) of a green fluorescent protein (GFP)-expressing vector in the VZ of wt and *COUP-TFI*$^{-/-}$ E14.5 brains (Fig. 2C). Slices from rostral to caudal regions of electroporated brains were analyzed after 4 days of culture in vitro (DIV). We observed a striking reduction of neurons reaching the CP principally from rostro- to caudomedial regions of mutant cortices (Fig. 2C-E; see Table S1 in the supplementary material). This defective migration was neither due to impairment of the glial scaffolding nor to abnormal specification of migrating neurons, because almost all GFP-positive cells failing to leave the IZ were Satb2-positive (UL) and Ctip2 (Bcl11b – Mouse Genome Informatics)-negative (deep layers) (see Fig. S2A-D in the supplementary material).

Notably, cell counting revealed a gradual increase in the percentage of GFP+ cells reaching the CP from rostral to caudal regions of wt cortices, with a maximum rate of migration in the caudomedial cortex (Fig. 2F). This migration gradient was lost in *COUP-TFI*$^{-/-}$ brains, although no differences were found between rostral- and caudal-most neocortical regions of wt and *COUP-TFI*$^{-/-}$ brains (Fig. 2F; see Table S1 in the supplementary material). To exclude any interference from the neurogenic gradient, we limited our statistical analysis of GFP+ cell distribution to the IZ and CP as well as to the lower, middle and upper regions within the CP (Fig. 2E; see Fig. S3A,B in the supplementary material). This analysis confirmed defective cell transition from the IZ to the CP in rostro- to caudomedial regions and showed a significant decrease in cells reaching the upper CP also in caudal-most slices. Analysis of cell migration within the CP also revealed impaired transition from lower to upper CP in rostromedial to caudal regions of *COUP-TFI*$^{-/-}$ cortices (see Fig. S3B in the supplementary material). Together, these data indicate that COUP-TFI regulates cell migration from IZ to CP in presumptive somatosensory and occipital cortex during mid-late corticogenesis.

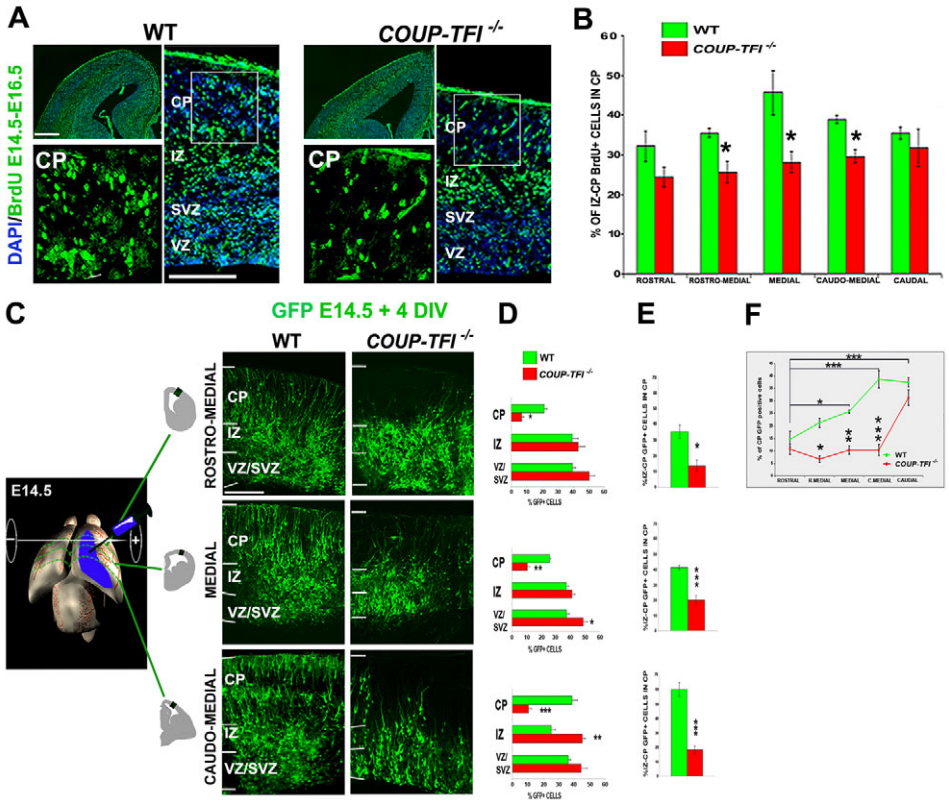

Fig. 2. Radial cell migration is impaired in *COUP-TFI*$^{-/-}$ mouse brains. (**A**) Immunostaining for BrdU of E16.5 medial coronal sections indicates decreased BrdU-positive cells in the CP of *COUP-TFI*$^{-/-}$ cortices. (**B**) Histogram showing the percentage of BrdU-positive cells migrating from the IZ to the CP from rostral to caudal regions of wt and mutant cortices (n=3). (**C**) Ex vivo electroporation of a GFP-expressing vector in E14.5 wt and *COUP-TFI*$^{-/-}$ neocortical VZ and organotypic slices from three distinct regions along the rostrocaudal axis after 4 days in culture (DIV). In diagrams to the left, black areas indicate the regions shown. (**D**) Histograms describing GFP-positive cells radial distribution in wt and *COUP-TFI*$^{-/-}$ brains (n=3). (**E**) Quantification of IZ/CP GFP-positive cells reaching the CP. (**F**) Line graph showing the percentage of GFP+ cells in the CP along the rostrocaudal axis of wt and *COUP-TFI*$^{-/-}$ brains (n=3). *P<0.05, **P<0.01, ***P<0.005. Scale bars: A (top left panel), 400 μm; A (right panel) and C, 200 μm.

Rnd2 rostrocaudal gradient is strongly altered in *COUP-TFI*$^{-/-}$ neocortex

We found that the small Rho-GTPase Rnd2, which we reported to be altered in *COUP-TFI*$^{-/-}$ brains (Armentano et al., 2006), is expressed in a high-rostral to low-caudal gradient, complementary to that of COUP-TFI (Fig. 3A) and to the migratory gradient (Fig. 2). Because Rnd2 normally modulates cell migration (Heng et al., 2008), we hypothesized that COUP-TFI represses *Rnd2* expression along the rostrocaudal axis. Indeed, we found that at E13.5, COUP-TFI inactivation abolished the *Rnd2* gradient and increased *Rnd2* expression in caudomedial cortical regions (Fig. 3B). Double labelling of E13.5 medial coronal sections with Tbr2 and *Rnd2* confirmed higher levels of *Rnd2* expression in the IZ, and more specifically in the CP, despite a normal distribution of basal progenitors (Fig. 3C).

At E15.5, when the majority of UL neurons are generated and start their migration to the CP, high levels of *Rnd2* expression were maintained in *COUP-TFI*$^{-/-}$ SVZ and IZ (Fig. 3D,E). Abnormal expression levels of *Svet1*, a marker of SVZ progenitors and multipolar-shaped cells (MSCs) (Sasaki et al., 2008; Tarabykin et al., 2001), and accumulation of Satb2+ cells were also observed in the SVZ and IZ of mutant brain adjacent sections, confirming that UL neurons, and more particularly CPNs, were properly specified but stalled as MSCs in the upper SVZ and IZ (Fig. 3E). Finally, *Rnd2* expression levels were still slightly higher in the deep cortex of *COUP-TFI*$^{-/-}$ brains at P0 (Fig. 3F). Taken together, our data indicate that the *Rnd2* gradient is abolished in *COUP-TFI*$^{-/-}$ brains and that *Rnd2* expression is increased in abnormally migrating cells.

COUP-TFI negatively regulates *Rnd2* expression through an Ngn2-independent pathway

In light of the role for Ngn2 in promoting *Rnd2* expression (Heng et al., 2008), we hypothesized that COUP-TFI and Ngn2 either regulate each other or act through independent pathways to fine-tune *Rnd2* expression. To distinguish between these two possibilities, we assessed *Rnd2* transcript levels relative to *Ngn2* and other factors shown to promote *Rnd2* expression (Heng et al., 2008). Despite the remarkable increase in *Rnd2* expression in E15.5 *COUP-TFI*$^{-/-}$ neocortices (57.9±7.8%, n=3, P=0.002), we found no significant changes in *Ngn2*, *NeuroD2* and *Tbr2* levels, and a mild decrease in *NeuroD1* expression (12.1±3.1%, n=3, P=0.02) (Fig. 4A; see Table S1 in the supplementary material). This suggests independent control of *Rnd2* by COUP-TFI. To confirm this hypothesis further, we generated double *COUP-TFI Ngn2* compound mutants (*dKO*). Interestingly, we found that in *dKO* brains *Rnd2* levels were increased in comparison with *Ngn2*$^{-/-}$ brains (Fig. 4B), indicating that repression of *Rnd2* expression by COUP-TFI occurs independently of Ngn2. This is confirmed further by the abnormally high levels of *Rnd2* in *COUP-TFIfl/fl*$^{Nex\text{-}Cre}$ brains (Fig. 2C), in which COUP-TFI is specifically inactivated in early post-mitotic cells (see Fig. S4 in the supplementary material).

Finally, by using MatInspector (Quandt et al., 1995) (http://www.genomatix.de/en/produkte/genomatix-software-suite.html), ECR browser (Loots and Ovcharenko, 2007) (http://ecrbase.dcode.org) and ChromAnalyzer (Montemayor et al., 2010), we identified five putative COUP-TFI binding sites at the *Rnd2* locus with variable evolutionary conservation in mammals (Fig. 4D). Two binding sites were very close and mapped in the *Rnd2* last intron (sites A, A1), whereas the other three mapped in the downstream genomic region of the *Rnd2* locus (sites B, C and D). Strikingly, site B mapped between the two previously identified E-boxes enhancing *Rnd2* expression in the developing cortex (Heng et al., 2008). To assess whether COUP-TFI binds to these sites in vivo, we performed chromatin immunoprecipitation (ChIP) on E14.5 telencephalic tissue with a COUP-TFI antibody (Tripodi et al., 2004). QPCR analysis of immunoprecipitated material showed enrichment of all five sites, although to different extents

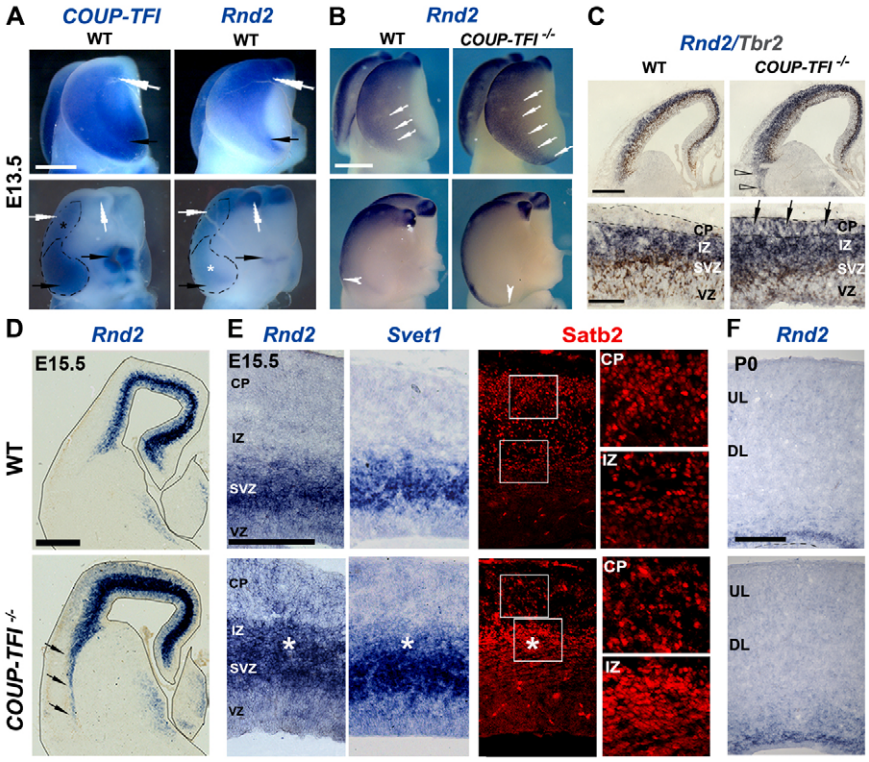

Fig. 3. Increased Rnd2 expression levels in *COUP-TFI*$^{-/-}$ mouse brains. (**A**) Dorsal and ventral views of E13.5 brains stained for *COUP-TFI* (black arrows) and *Rnd2* (white arrows). The dashed line demarcates *COUP-TFI*-positive territories. (**B**) In *COUP-TFI*$^{-/-}$ brains, expression of *Rnd2* in caudal-most regions is increased (arrows in lateral views and arrowheads in ventral views). (**C**) Double labelling for Tbr2 protein and *Rnd2* of E13.5 medial coronal sections indicates increased *Rnd2* expression in mutant SVZ and IZ, and ectopic expression in the CP (black arrows) and lateroventral cortex (open arrowheads). (**D**) Coronal sections shows increased *Rnd2* expression in dorsal and ventral E15.5 *COUP-TFI*$^{-/-}$ neocortex (black arrows). (**E**) *Rnd2* and *Svet1* transcript enhancement and Satb2+ cell accumulation in the mutant IZ of adjacent E15.5 coronal sections (asterisks and high magnification views). (**F**) Rnd2 expression in wt and mutant P0 coronal sections. UL, upper layers; DL, deep layers. Scale bars: A,B, 1 mm; C (top left panel), 200 μm; C (bottom left panel), 100 μm; D, 800 μm; E,F, 200 μm.

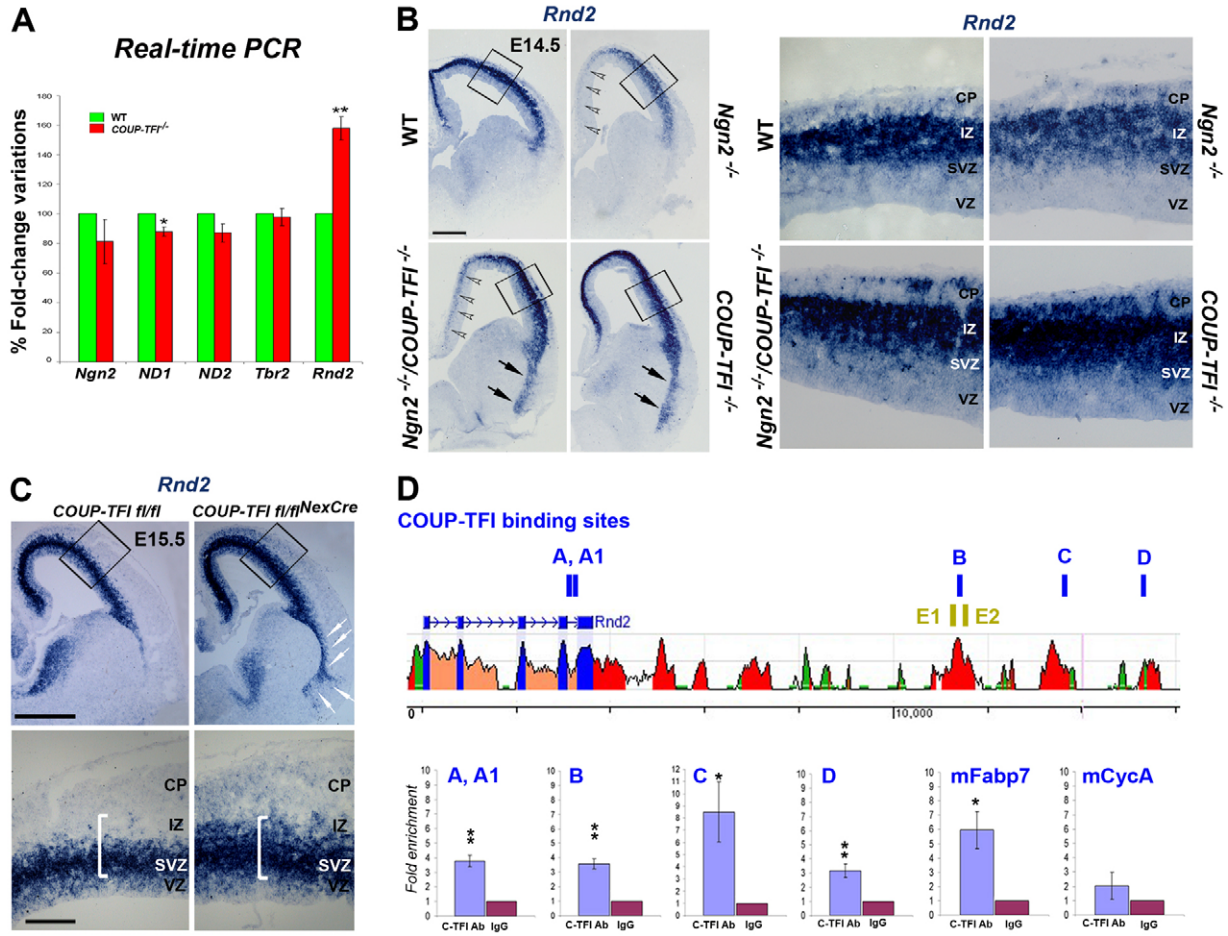

Fig. 4. COUP-TFI represses *Rnd2* expression post-mitotically in an Ngn2-independent manner. (**A**) Histogram showing no significant changes in *Ngn2*, *Tbr2*, *NeuroD1* (*ND1*) and *NeuroD2* (*ND2*) expression in *COUP-TFI*$^{-/-}$ mouse cortices despite the strong increase in *Rnd2* expression. (**B**) *Rnd2* expression decreases in *Ngn2*$^{-/-}$ neocortex and archicortex (open arrowheads) and is rescued to normal levels in *COUP-TFI*$^{-/-}$;*Ngn2*$^{-/-}$ (*dKO*) neocortex. Ectopic expression of *Rnd2* in lateroventral neocortex of *COUP-TFI* and double *KO* brains (black arrows). Right-hand panels show high magnification views of boxed areas in the left-hand panels. (**C**) In *COUP-TFIfl/fl*^{NexCre} E15.5 coronal sections, in which COUP-TFI is inactivated post-mitotically, *Rnd2* expression is strongly enhanced (bracket in lower panels) and ectopically detected in the CP and ventral cortex (arrows). Lower panels are magnifications of boxed areas in upper panels. (**D**) Snapshot from ECR browser showing the conservation of COUP-TFI binding sites (A, A1, B, C, D) along the *Rnd2* locus. Immunoprecipitation of chromatin (ChIP) from E14.5 wt embryos indicates that COUP-TFI binds these sites with different affinities (n=3). E1 and E2 are previously identified *Rnd2* enhancers. mFabp7 and mCycA sites are positive and negative controls, respectively. All data are expressed as 'relative' fold enrichment and normalized against ChIP performed on the same samples with an anti-Dicer antibody. *P<0.05, **P<0.01. Scale bars: 400 μm.

(Fig. 4D; see Table S1 in the supplementary material), suggesting that COUP-TFI binds to these sequences with different affinities. Together, our data strongly suggest a direct repression of *Rnd2* by COUP-TFI in post-mitotic late-born cortical neurons.

Loss of COUP-TFI function alters morphology of migrating cells

Next, we carefully assessed the morphology of migrating GFP+ cells in wt and *COUP-TFI*$^{-/-}$ medial brain slices at the sites where *Rnd2* expression is highly increased (Fig. 5A) and observed a significant increase of MSCs in mutant IZ (Fig. 5B; wt: 39.4±2.1%, n=3; *KO*: 59.1±1.8%, n=4; P<0.005), although their radial distribution along the neocortex was unchanged compared with wt brains (Fig. 5C; see Table S1 in the supplementary material). Accordingly, the BSC percentage decreased from 59.3±1.7% in wt to 38.8±2.1% in *COUP-TFI*$^{-/-}$ brains (P<0.005) (Fig. 5B), whereas no alterations were observed in the percentage of round-shaped cells (RSCs, another morphology adopted by migrating neurons) (see Table S1 in the supplementary material). We observed an abnormal BCS distribution along the radial extent of the cortex. Normally, the highest percentage of BSCs is found in the upper IZ and the CP; however, mutant BSCs were mainly located in the IZ (Fig. 5C), indicating that although they adopt a bipolar morphology, *COUP-TFI*$^{-/-}$ neurons fail to reach the CP. Thus, our data indicate that COUP-TFI is required for both the morphological transition from multipolar to bipolar shape and the intrinsic migratory property of BSCs within the IZ and CP during UL neuron radial migration.

Rnd2 downregulation rescues the distribution and morphological defects of *COUP-TFI*-deficient neurons

To test whether abnormally high levels of *Rnd2* expression causes the migratory and morphological defects observed in *COUP-TFI*$^{-/-}$ brains, we reduced *Rnd2* expression levels by

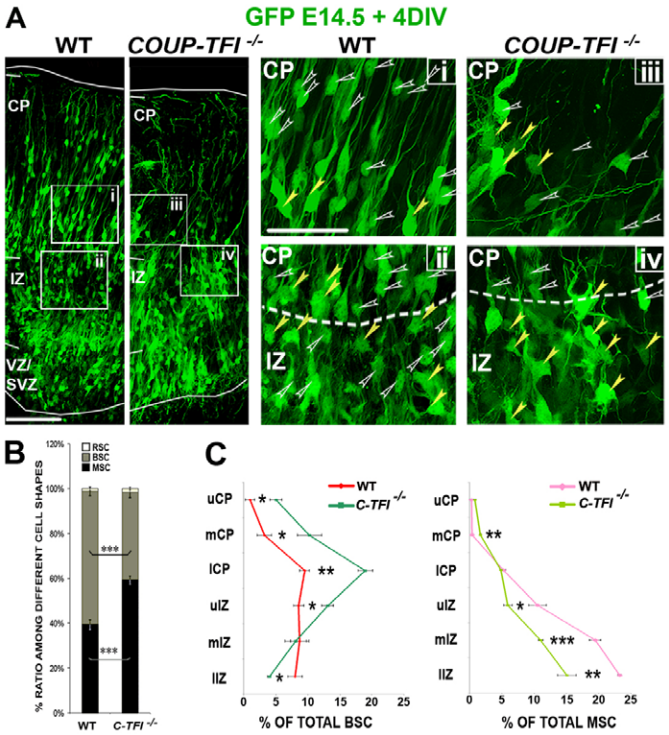

Fig. 5. Abnormal morphology and distribution of migrating cells in *COUP-TFI*$^{-/-}$ mouse brains. (**A**) Ex vivo electroporation of a GFP-expressing vector in the VZ of E14.5 neocortices. After 4 days of organotypic culture (4 DIV) multipolar-shaped cells (MSCs, yellow arrowheads) accumulate in the mutant IZ. (Ai-iv) High magnification views of boxed areas in A. Dashed line indicates boundary of CP and IZ. (**B**) The ratio of MSCs is increased at the expense of bipolar shaped cells (BSCs, open arrowheads in A) in *COUP-TFI*$^{-/-}$ neocortices (n=3). No changes were found in the percentage of round shaped cells (RSCs). (**C**) Distribution of MSCs and BSCs along the radial extent of the neocortex indicates that the majority of mutant BSCs are stalled in the IZ and lower CP (lCP), whereas mutant MSCs accumulate principally in the IZ (n=3). uCP, upper CP; mCP, middle CP; uIZ, upper IZ; mIZ, middle IZ; lIZ, lower IZ. *P<0.05, **P<0.01, ***P<0.005. Scale bar: 100 μm.

electroporation of two *Rnd2*-specific *shRNA–IRES-GFP* expressing vectors (noted *SH1* and *SH2* below) (Fig. 6; see Fig. S5A in the supplementary material) (Heng et al., 2008). As a control we used a scrambled *shRNA* (*SCR*). In P19 cells, a strong silencing effect on Rnd2 protein expression was observed with both *sh-RNAs*, although they exhibited different efficacies (see Fig. S5A in the supplementary material). Electroporation of *SH2* in mutant cortices resulted in a remarkable rescue of the number of GFP+ mutant cells reaching the CP (Fig. 6A,B; *NULL-SCR*: 4.1±0.2%, n=3; *NULL-SH2*: 19.8±1.6%; n=4; P<0.001) and, within the CP, in the upper cortical region (*NULL-SCR*: 2.3±1.2%; *NULL-SH2*: 14.0±0.9%; P=0.003) (Fig. 6A,B). *SH1* electroporation instead resulted in a mild decrease in the number of mutant GFP+ cells in the VZ/SVZ compared with mutant *SCR*-expressing cells. However, mutant *SH1*+ cells accumulated in the IZ and failed to reach the CP (Fig. 6A,B; see Table S1 in the supplementary material). *SH2* was, thus, more effective in rescuing mutant cell transition from VZ/SVZ to CP (Fig. 6B; see Table S1 in the supplementary material), possibly because *Rnd2* levels were approximately restored to normal. Conversely, *SH1* reduced *Rnd2* expression, both in wt and mutant cells, below a critical threshold leading to poor migratory rescue (see Fig. S5A-C and Table S1 in the supplementary material).

Next, we assessed whether rescued GFP+ cells re-acquired their correct shape during migration. The number of MSCs significantly decreased in *SH2*-electroporated *COUP-TFI*$^{-/-}$ cortices, whereas there was a significant and concomitant increase of BSCs (Fig. 6C; *NULL-SCR*, MSC: 66.5±1.8%, BSC: 31.4±1.2%, n=3; *NULL-SH2*, MSC: 54.3±1.7%, BSC: 43.8±1.7%, n=4; P<0.05). Furthermore, mutant BSC radial distribution was, remarkably, rescued by *SH2* electroporation, whereas no changes were observed in the localization of *SH2*+ mutant MSCs (Fig. 6D; see Fig. S5D and Table S1 in the supplementary material). Our findings strongly support a role for COUP-TFI, via the regulation of Rnd2, in promoting transition from MSC to BSC and in controlling correct distribution of BSCs in the IZ and CP during migration of late-born neurons.

Callosal axonal extension and dendritic morphology of CPNs are dependent on proper *Rnd2* expression levels

Next, to assess whether migratory impairment would affect CPN maturation, we inactivated COUP-TFI in single migrating neurons via in utero electroporation of a *Cre-IRES-GFP*-expressing vector (referred to as *CRE*) in E14.5 *COUP-TFI*$^{flox/flox}$ (*floxed*) mice. To rescue any eventual morphological defect in mutant neurons we co-electroporated *SCR*- or *SH2* together with *CRE*. Analysis of Cre expression in electroporated brains at E18.5 confirmed that COUP-TFI was inactivated in single Cre-positive cells of *floxed* mice and that *CRE* electroporation did not cause cell death (see Fig. S6A-C in the supplementary material). Thus, GFP-expressing cells could be followed as individual migrating cells extending their axons in a wild-type environment (Fig. 7).

Acute inactivation of COUP-TFI resulted in a significant decrease of GFP+ neurons reaching the upper CP at E18.5 in *floxed* brains (Fig. 7A,B; $wt_{CRE/SCR}$: 54.8±2.3%; $fl/fl_{CRE/SCR}$: 35.4±0.8%; n=4; P<0.005). The migratory defect of mutant cells was partially rescued by co-electroporation of *SH2* and *CRE* in *floxed* brains ($fl/fl_{CRE/SCR}$: 35.4±0.8%; $fl/fl_{CRE/SH2}$: 43.7% ± 2.4%; n=4, P<0.05) (Fig. 7A,B; see Table S1 in the supplementary material), indicating that COUP-TFI acts cell-autonomously through Rnd2 to control migratory properties. Moreover, *CRE*/*SCR*-electroporated *floxed* brains showed a strong impairment in the elongation of callosal axons, which failed to reach the midline as a compact fibre tract (Fig. 7C; n=4). Remarkably, co-electroporation of *CRE* and *SH2* in *floxed* brains rescued the midline crossing by GFP+ callosal axons (Fig. 7C), strongly indicating an important role for Rnd2 in axonal extension.

To assess whether mutant callosal axon elongation was permanently arrested or just delayed, we repeated the above experiment and collected brains at P8. We observed that both wt and mutant GFP+ callosal projections were able to reach the contralateral cortex (Fig. 7D). As it is not possible to quantify the percentage of crossing fibres in electroporated brains owing to the variability in the number of cells incorporating GFP, we analyzed the extension and volume of the callosal commissure in *COUP-TFIflox/flox*^{Emx1Cre} adult brains (Armentano et al., 2007). Interestingly, we found that the rostrocaudal extension and total volume of the callosal commissure were reduced to 70.7±3.8% and 63.0±7.1%, respectively, in *COUP-TFI* conditional adult brains (see Fig. S7 in the supplementary material), suggesting that most callosal axons are just delayed in crossing the midline after

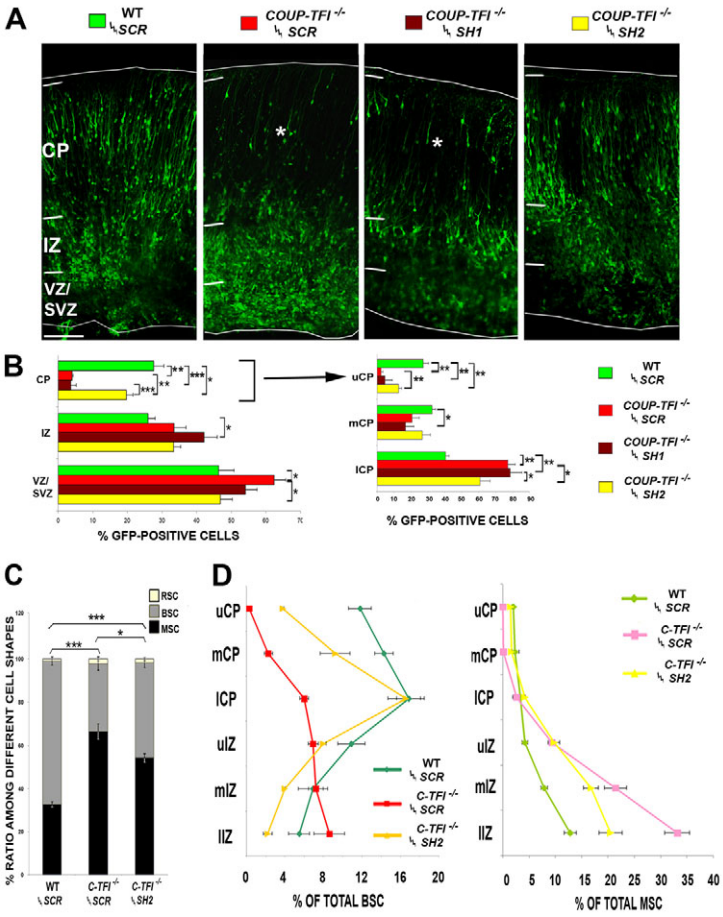

Fig. 6. Lowering Rnd2 expression levels in *COUP-TFI*$^{-/-}$ mice rescues impaired neuronal radial migration. (**A**) Wt and *COUP-TFI*$^{-/-}$ brains were electroporated with a control (*SCR*; *n*=3) and two different *Rnd2*-specific *shRNA-IRES-GFP* expressing vectors (*SH1* and *SH2*; *n*=4). *SH1* does not appreciably recover neuronal migration with respect to mutant brains electroporated with *SCR* (asterisks in CP). *SH2* rescues radial migration. (**B**) Histogram of the experiments described in A. (**C**) Lowering of *Rnd2* levels partially rescues the defective multipolar (MSC) to bipolar (BSC) shape transition of mutant cells (wt, *null SCR n*=3; *null SH2 n*=4). (**D**) Radial distribution of mutant BSCs is rescued by *SH2* (yellow) with respect to the *SCR*+ mutant neurons, whereas no relevant changes are observed in the distribution of *SH2*+ MSC (wt, *null SCR n*=3; *null SH2 n*=4). See Table S1 in the supplementary material for statistical analysis of data. uCP, upper CP; mCP, middle CP; lCP, lower CP; uIZ, upper IZ; mIZ, middle IZ; lIZ, lower IZ. **P*<0.05, ***P*<0.01, ****P*<0.005. Scale bars: A, 100 μm.

inactivation of COUP-TFI. Whereas callosal axons normally arborize in layers II/III of contralateral somatosensory regions (S1 and S2) at P8 (Wang et al., 2007) (Fig. 7Di,ii,vii), mutant callosal axons showed poor arborization in these regions (Fig. 7Diii,iv,viii). Strikingly, in *SH2*-electroporated *floxed* brains, GFP+ axon innervation of contralateral parietal areas was partially rescued, particularly in S2 (Fig. 7Dv,vi,ix).

In wt control brains, Satb2-positive callosal neurons had a branched apical dendrite and complex apical tufts in layer I at P8 (Fig. 8A). Although the cell-autonomous inactivation of *COUP-TFI* strongly affected the morphology of these tufts, which barely reached the marginal zone (MZ) (Fig. 8A,B; see Fig. S8A,B and Movies 1 and 2 in the supplementary material), the *floxed CRE/SH2*-electroporated neurons restored proper contact with the pial surface and apical tuft complexity in layer I (Fig. 8A,B; see Fig. S8A,B and Movie 3 in the supplementary material). However, either mutant or *SH2*-rescued mutant neurons abnormally aggregated in small clusters in deep positions, which were never observed for wt neurons (Fig. 8A; see Fig. S8B,C in the supplementary material). Finally, dendrite branching, strongly altered in *SCR*-expressing mutant neurons, was also rescued in *SH2*-electroporated mutant neurons (Fig. 8B; see Fig. S8A in the supplementary material), although the dendrite length was increased in *COUP-TFI*-deficient neurons ($wt_{CRE/SCR}$: 193.9±12.1 μm; $fl/fl_{CRE/SCR}$: 287.3±31.2 μm; *n*=3; *P*<0.05) but not restored in *CRE*/*SH2*-electroporated brains ($wt_{CRE/SCR}$: 193.9±12.1 μm; $fl/fl_{CRE/SH2}$: 285.9±5.4 μm; *n*=3; *P*<0.005) (see Fig. S8D in the supplementary material). Taken together, our analyses demonstrate a cell-autonomous role for COUP-TFI in migration, targeting, and axonal and dendritic arborization of CPNs and indicate that fine-tuning of *Rnd2* levels by COUP-TFI during radial migration favours CPN maturation.

DISCUSSION

COUP-TFI and Ngn2 independently promote radial migration by fine-tuning *Rnd2* levels

Our data contribute to the delineation of a genetic circuitry underlying *Rnd2* expression during glia-guided radial migration and confirms that the fine control of its expression during different phases of this process is crucial for correct radial distribution of UL newborn neurons. We demonstrate that the sharp decrease of *Rnd2* in the upper IZ favours glia-guided BSC migration to the CP. We demonstrate that COUP-TFI represses *Rnd2* expression levels in the IZ independently of its main activator (Ngn2) in post-mitotic migrating neurons, indicating a direct role of COUP-TFI during early phases of glia-guided radial migration. Moreover, we show that COUP-TFI binds directly to various *Rnd2* downstream sequences, probably recruiting chromatin remodelling factors or other co-repressors (Montemayor et al., 2010; Nishihara et al., 2004; Zhang et al., 2009). Strikingly, one of the COUP-TFI binding sites is positioned between two Ngn2-bound sequences in a transcriptional enhancer previously identified in the downstream region of the *Rnd2* locus (Heng et al., 2008). COUP-TFI might thus prevent or destabilize the binding of Ngn2 and other basic helix-loop-helix (bHLH) factors to the *Rnd2* enhancer in the IZ.

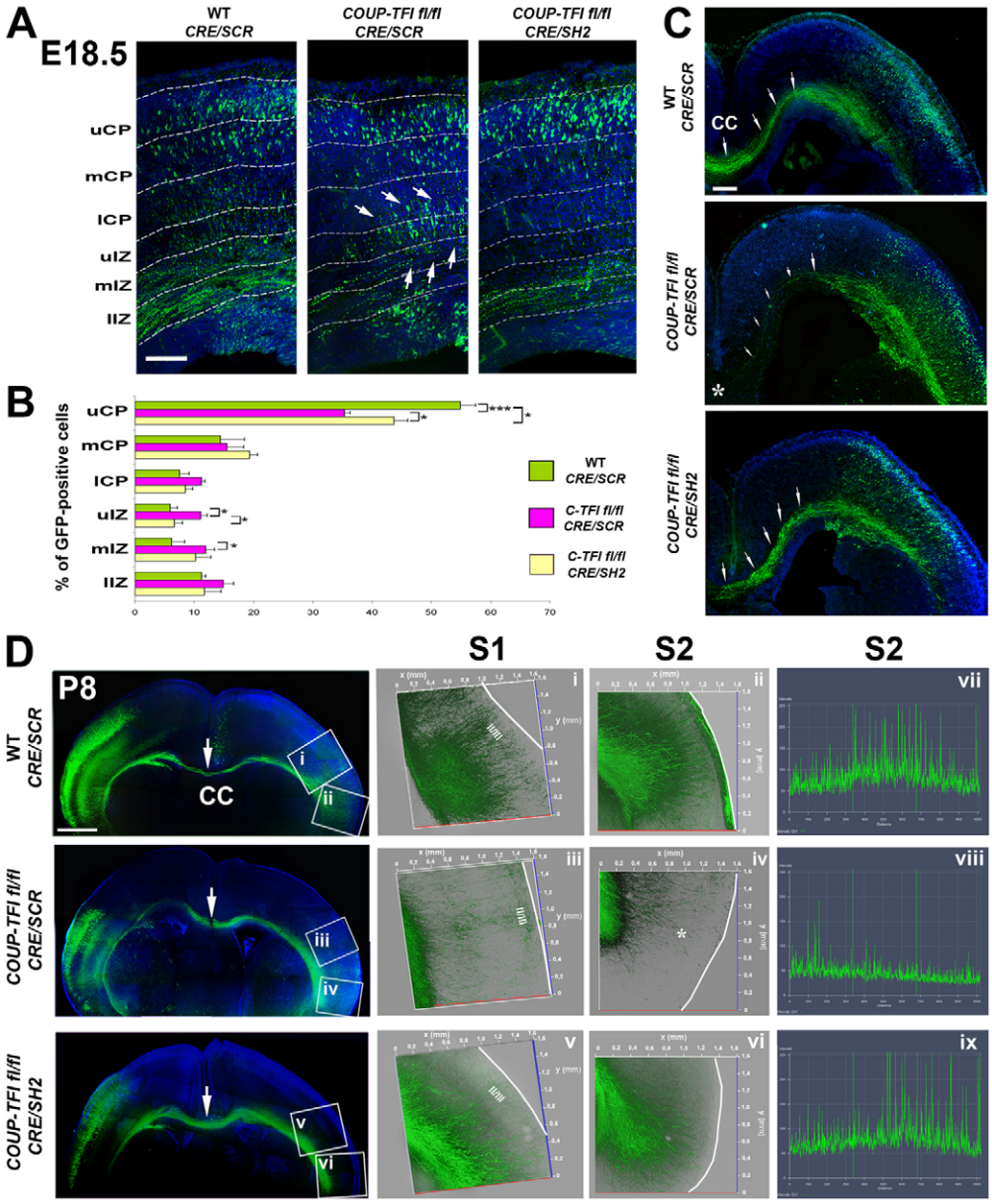

Fig. 7. COUP-TFI-deficient CPNs show defective axonal elongation and arborization, which is cell-autonomously rescued by lowering Rnd2 expression. (**A**) Acute deletion of *COUP-TFI* in single migrating neurons by in utero co-electroporation of a Cre-expressing vector with either a control or Rnd2-specific *shRNA*-expressing vectors (*SCR* and *SH2*, respectively) in the lateral cortex of E14.5 wt and *COUP-TFIflox/flox* mouse brains. *SCR*+ mutant neurons show altered migration at E18.5 (arrows). Affected migration is partially rescued by *CRE/SH2* co-electroporation. (**B**) Quantification of the experiments described in A (n=4). Dashed lines indicate boundaries between subcompartments. (**C**) *CRE/SCR* expressing *floxed* CPNs, in contrast to *CRE/SCR*+ wt neurons, fail to project their axons towards the midline (arrows and asterisk) (n=3). Callosal axons from *SH2*-rescued mutant CPNs elongate properly and cross the midline (arrows) (n=3). (**D**) P8 wt and *COUP-TFIflox/flox* coronal slices from brains co-electroporated at E14.5 either with *CRE/SCR* or with *CRE/SH2*, as described in A. Arrows indicate crossing of GFP-positive callosal axons. (Di-vi) Details of cortical regions corresponding to somatosensory areas 1 and 2 (S1, S2) of electroporated brains elaborated by *Transparent* plug-in (Zeiss ZEN Confocal Software). (Di-ii) 3D images show almost complete innervation of wt contralateral cortex by callosal axons. (Diii-iv) GFP+ mutant axons poorly innervate contralateral S1 and S2 regions. (Dv-vi) A remarkable rescue of mutant axon arborization in S2 and a partial recovery of their innervation in S1 (limited to deeper regions) of the contralateral cortex is obtained after *CRE/SH2* co-electroporation. (Dvii-ix) Quantification of GFP intensity in lateroventral cortex (S2 region) from wt and *COUP-TFI* floxed brains obtained by *Profile* plug-in (Zeiss ZEN Confocal Software) confirms poor innervation in S2 of *CRE/SCR*-electroporated floxed axons, which is recovered after *CRE/SH2* co-electroporation. **P*<0.05, ****P*<0.005. Scale bars: A, 200 μm; C, 300 μm; D, 900 μm.

This finding correlates with a previous study showing that Ngn2 overexpression does not alter radial distribution of migrating cells in this compartment (Hand et al., 2005). Overall, our data demonstrate that Ngn2 and COUP-TFI are independently involved in the fine-tuning of *Rnd2* expression and indicates that COUP-TFI normally promotes glia-guided radial migration by progressively repressing *Rnd2* expression along medial and caudal regions of the neocortex during mid- to late corticogenesis.

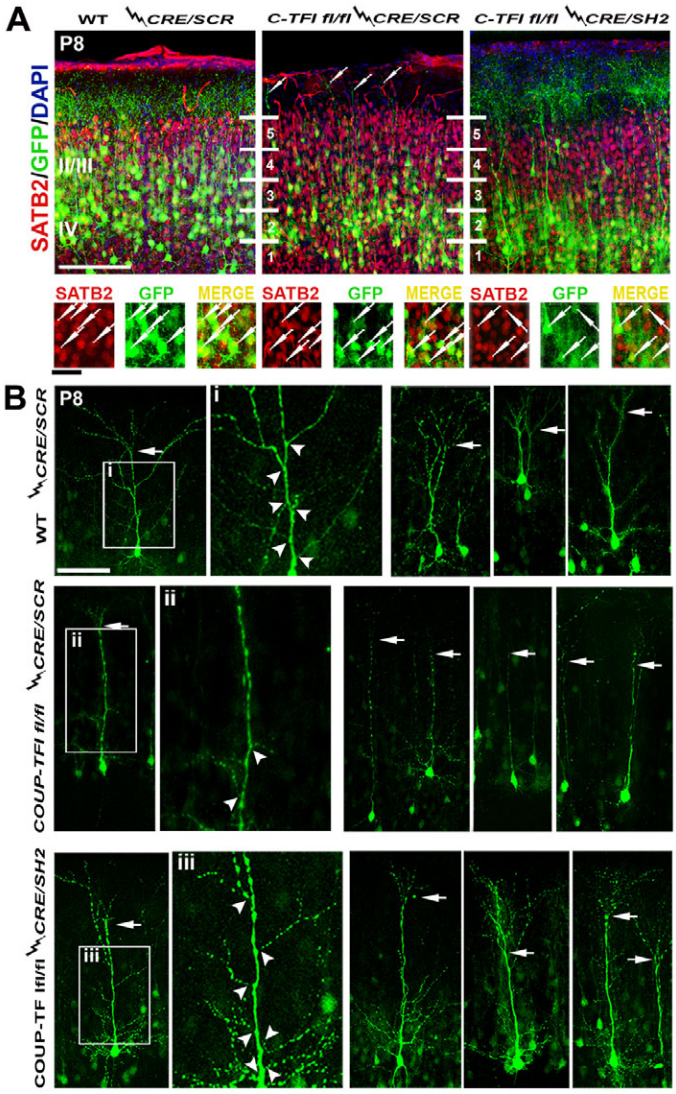

Fig. 8. Impaired dendritic morphology of *COUP-TFI*-deficient pyramidal neurons in mouse is rescued by lowering *Rnd2* levels. (**A**) The apical tuft morphology of P8 *COUP-TFIflox/flox* callosal neurons co-electroporated in utero at E14.5 with *Cre*- and control *shRNA-IRES-GFP*-expressing vectors (*CRE* and *SCR*) is strongly impaired (arrows). This defect was remarkably rescued by co-electroporation of *CRE* and *Rnd2*-specific *shRNA-IRES-GFP*-expressing vector 2 (*SH2*). Lower panels show high magnified details of upper panels showing that GFP+ pyramidal neurons correctly expressed Satb2 in all three conditions (arrows). Numbers 1-5 indicate arbitrary division of UL into five bins (see Fig. S8C in the supplementary material). (**B**) *CRE/SCR*-expressing wt pyramidal neurons at P8 have a branched apical dendrite (white arrowheads in Bi) with a complex shaped apical tuft (white arrows). COUP-TFI-deficient neurons show a thin and almost unbranched apical dendrite with no or simple apical tufts (Bii). Co-electroporation of *SH2* with *CRE* in *COUP-TFI-floxed* neurons restores their defective morphology (Biii). **P*<0.05, ***P*<0.001. Scale bars: A (top left panel), 200 μm; A (bottom left panel) 50 μm; B, 100 μm.

A graded rate of migration along the rostrocaudal axis might regulate important processes of corticogenesis

In this report, we show that the expression of the atypical Rho-GTPase *Rnd2* follows a high-rostral to low-caudal gradient, which is complementary to the one described for COUP-TFI (Armentano et al., 2007; Liu et al., 2000; Tomassy et al., 2010; Zhou et al., 2001). This gradient is also complementary to the UL neurons migratory gradient detailed in this study. Thus, high expression levels of *Rnd2* in rostral cortex might restrict migrating cells from reaching the CP more than in caudal regions. In the absence of COUP-TFI function, the *Rnd2* gradient is abolished and higher *Rnd2* expression levels are detected caudally. Accordingly, a lower percentage of cells reach the cortical plate. Thus, our data, together with previous reports, demonstrate that *Rnd2* expression is downregulated by increasing levels of COUP-TFI along the rostrocaudal axis, leading to differential rates of migration from rostral to caudal regions of the cortex.

The biological meaning of this migratory gradient is still unclear and deserves further investigation. However, other factors involved in cortical arealization, besides COUP-TFI, seem to modulate neuron radial migration (O'Leary et al., 2007). Furthermore, neurons in ULs (and particularly in layer IV) represent a source of signals for thalamocortical innervation (Shimogori and Grove, 2005), an important process refining cortical arealization. It is thus tempting to hypothesize that COUP-TFI might, at least in part, control the topography of thalamocortical innervation by modulating the timing of neuronal migration to layer IV along the rostrocaudal axis of the neocortex.

Accurate Rnd2 expression levels promote proper dendritic morphology of callosal pyramidal neurons

Here, we also provide evidence that COUP-TFI is involved in the development of correct dendritic morphology of UL neurons. The precise morphology of these neurons could be controlled during early phases of pyramidal neuron radial migration. A previous report suggested that initial apical dendrite formation occurs during early stages of glia-guided radial migration and that RhoA activity inhibits this process by promoting MSC morphology (Hand et al., 2005). As Rnd2 modulates RhoA activity via pragmin interaction (Pacary et al., 2011; Tanaka et al., 2006), higher Rnd2 expression levels observed in *COUP-TFI* mutants might alter RhoA activity and thus disrupt the formation of the initial dendrite, ultimately leading to an increased number of MSCs. Our data suggest that altered initial dendritic formation might also affect late dendritic arborization of pyramidal neurons. However, although lowering *Rnd2* levels in mutant neurons restores late dendritic complexity, it only partially rescues the morphological transition from MSC to BSC, indicating that most rescued cells were defective BSCs stalled in the IZ and lower CP regions. We cannot exclude that our *shRNA* strategy failed to re-establish precise levels of *Rnd2*; however, our results are consistent with previous data showing that artificially enhanced *Rnd2* levels only lead to a slight increase in MSC (Heng et al., 2008).

Another possibility is that the development of an abnormal apical dendrite with no or few apical tufts, as observed in *COUP-TFI*-deficient neurons, might be due to the failure of their leading process to reach the MZ and activate reelin-mediated dendritic branching (Hunter-Schaedle, 1997; Niu et al., 2004; Ohshima et al., 2007; Sanada et al., 2004). It has been shown previously that reelin in the MZ stabilizes the leading process by cofilin phosphorylation (Chai et al., 2009). Lack of proper stabilization of the leading process might not only affect final phases of radial migration but also dendritic maturation. Thus, the remarkable rescue of dendritic complexity observed in *SH2*-rescued *COUP-TFI*-deficient CPNs might be due to restored contact of the MZ by their leading

processes. Nevertheless, although rescued *COUP-TFI*-deficient dendrites successfully target the MZ, both mutant and *SH2*-rescued mutant cells remain beneath the upper CP with abnormally long apical dendrites and form abnormal cell clusters in the ULs. We suggest that these processes might be independent from *Rnd2* as it was already reported that the expression of two microtubule-associated proteins, MAP1B (Mtap1b – Mouse Genome Informatics) and MAP2 (Map2 – Mouse Genome Informatics), strongly decreases in COUP-TFI-deficient dendrites (Armentano et al., 2006), whereas cell adhesion increases in the absence of COUP-TFI function (Adam et al., 2000). Furthermore, *Rnd2* expression in the CP seems to be very low during late stages of corticogenesis.

Thus, correct positioning of UL neurons does not seem to be a prerequisite for the acquisition of proper dendritic morphology. However, correct timing in reaching the CP, and more particularly the MZ, might be crucial for late-born migrating neurons to acquire a fully mature morphology.

COUP-TFI promotes BSC radial migration and callosal axon elongation by repressing Rnd2

Beside dendritic abnormalities, COUP-TFI-deficient callosal pyramidal neurons show delayed axonal elongation and impaired contralateral innervation. Although previous studies suggested a link between neuron radial migration and CC formation, a direct relationship between proper cell migration and callosal neuron differentiation has not been fully established (Donahoo and Richards, 2009; Richards et al., 2004). Inactivation of various molecules involved in radial migration, such as Dcx and Dclk, leads to affected migration and defective commissural outgrowth (Deuel et al., 2006; Koizumi et al., 2006); however, their expression is maintained at high levels in the CP during late events of differentiation. In this study, we show that altered callosal neuron migratory properties in *COUP-TFI null* mice correlate with a strong delay in callosal axon midline crossing at perinatal stages as well as reduced arborization at P8. In accordance with previous observations suggesting that axon elongation starts during BSC migration (Hatanaka and Murakami, 2002; Noctor et al., 2004; Norris and Kalil, 1991), we observed altered distribution of mutant BSCs along the IZ and CP and delayed callosal axon elongation, which were both restored by lowering *Rnd2* levels in mutant neurons. Accordingly, a previous study demonstrated that the interaction of Rnd2 with plexin D1 inhibits neurite outgrowth in cortical neurons (Uesugi et al., 2009). Finally, because Rnd2 modulates actin dynamics through interaction with the WASP proteins (Kakimoto et al., 2004), it is highly possible that increased Rnd2 levels might alter BSC neurite outgrowth, a process that is at the base of both glia-guided migration and CC formation.

Finally, in light of its expression gradient, we propose that Rnd2 might play an important role in CC formation by modulating the axonal elongation rate along the rostrocaudal axis of the neocortex. Previous studies demonstrated that all components of the CC (rostral, medial and caudal) cross the midline at similar developmental stages. As the midline allows callosal axon crossing mainly in the anterior half of the medial cortex and only for a restricted time, caudal callosal axons should cover greater distances to reach the crossing site and their homotypic regions (Richards et al., 2004). One can thus speculate that caudomedial and caudal CPNs that express lower levels of Rnd2 during migration, elongate their axons at a higher rate to reach the crossing regions at the correct time.

In conclusion, our study clearly demonstrates that COUP-TFI repression of Rnd2 in the IZ is crucial for proper migration of late-born BSC neurons. This suggests that progressive lowering of Rnd2 levels along the rostrocaudal cortical axis modulates the timing of CPN settlement as well as the rate of callosal axon elongation in different regions of the neocortex, ultimately favouring CC formation.

Acknowledgements

We would like to thank V. Tarabykin for the *Svet1* plasmid and Satb2 polyclonal antibody; M. Nieto for the *Cux1* and *Cux2* plasmids; R. Hevner for the Tbr1 antibody; G. Andolfi for genotyping; M. Giordano for animal husbandry; D. Di Nucci and G. Esposito for surgical assistance; and S. Arbucci, and F. A. Martín for confocal imaging. We are very thankful to R. Rispoli and the TIGEM Bioinformatics Core; and particularly to F. A. Pereira and C. Montemayor for the ChromAnalyzer-driven bioinformatic analysis of the *Rnd2* locus; to J. Hazan for critical reading; and to members of the Studer laboratory for fruitful discussions.

Funding

This work was supported by the Italian Telethon Foundation [TMSC24TELB to M.S.]; the 'Compagnia di San Paolo', Program of Neuroscience [TMSP14CSPA to M.S.]; and the L'Agence nationale de la recherche Chaire d'Excellence Program [R09125AA to M.S.].

Competing interests statement

The authors declare no competing financial interests.

Supplementary material

Supplementary material for this article is available at
http://dev.biologists.org/lookup/suppl/doi:10.1242/dev.068031/-/DC1

References

Aboitiz, F., Morales, D. and Montiel, J. (2003). The evolutionary origin of the mammalian isocortex: towards an integrated developmental and functional approach. *Behav. Brain Sci.* **26**, 535-552.

Adam, F., Sourisseau, T., Metivier, R., Le Page, Y., Desbois, C., Michel, D. and Salbert, G. (2000). COUP-TFI (chicken ovalbumin upstream promoter-transcription factor I) regulates cell migration and axogenesis in differentiating P19 embryonal carcinoma cells. *Mol. Endocrinol.* **14**, 1918-1933.

Alcamo, E. A., Chirivella, L., Dautzenberg, M., Dobreva, G., Farinas, I., Grosschedl, R. and McConnell, S. K. (2008). Satb2 regulates callosal projection neuron identity in the developing cerebral cortex. *Neuron* **57**, 364-377.

Armentano, M., Filosa, A., Andolfi, G. and Studer, M. (2006). COUP-TFI is required for the formation of commissural projections in the forebrain by regulating axonal growth. *Development* **133**, 4151-4162.

Armentano, M., Chou, S. J., Srubek Tomassy, G., Leingartner, A., O'Leary, D, D. and Studer, M. (2007). COUP-TFI regulates the balance of cortical patterning between frontal/motor and sensory areas. *Nat. Neurosci.* **10**, 1277-1286.

Bellenchi, G. C., Gurniak, C. B., Perlas, E., Middei, S., Ammassari-Teule, M. and Witke, W. (2007). N-cofilin is associated with neuronal migration disorders and cell cycle control in the cerebral cortex. *Genes Dev.* **21**, 2347-2357.

Britanova, O., de Juan Romero, C., Cheung, A., Kwan, K. Y., Schwark, M., Gyorgy, A., Vogel, T., Akopov, S., Mitkovski, M., Agoston, D. et al. (2008). Satb2 is a postmitotic determinant for upper-layer neuron specification in the neocortex. *Neuron* **57**, 378-392.

Chai, X., Forster, E., Zhao, S., Bock, H. H. and Frotscher, M. (2009). Reelin stabilizes the actin cytoskeleton of neuronal processes by inducing n-cofilin phosphorylation at serine3. *J. Neurosci.* **29**, 288-299.

Cubelos, B., Sebastian-Serrano, A., Beccari, L., Calcagnotto, M. E., Cisneros, E., Kim, S., Dopazo, A., Alvarez-Dolado, M., Redondo, J. M., Bovolenta, P. et al. (2010). Cux1 and Cux2 regulate dendritic branching, spine morphology, and synapses of the upper layer neurons of the cortex. *Neuron* **66**, 523-535.

Deuel, T. A., Liu, J. S., Corbo, J. C., Yoo, S. Y., Rorke-Adams, L. B. and Walsh, C. A. (2006). Genetic interactions between doublecortin and doublecortin-like kinase in neuronal migration and axon outgrowth. *Neuron* **49**, 41-53.

Donahoo, A. L. and Richards, L. J. (2009). Understanding the mechanisms of callosal development through the use of transgenic mouse models. *Semin. Pediatr. Neurol.* **16**, 127-142.

Dulabon, L., Olson, E. C., Taglienti, M. G., Eisenhuth, S., McGrath, B., Walsh, C. A., Kreidberg, J. A. and Anton, E. S. (2000). Reelin binds alpha3beta1 integrin and inhibits neuronal migration. *Neuron* **27**, 33-44.

Englund, C., Fink, A., Lau, C., Pham, D., Daza, R. A., Bulfone, A., Kowalczyk, T. and Hevner, R. F. (2005). Pax6, Tbr2, and Tbr1 are expressed sequentially by radial glia, intermediate progenitor cells, and postmitotic neurons in developing neocortex. *J. Neurosci.* **25**, 247-251.

Faedo, A., Tomassy, G. S., Ruan, Y., Teichmann, H., Krauss, S., Pleasure, S. J., Tsai, S. Y., Tsai, M. J., Studer, M. and Rubenstein, J. L. (2008). COUP-TFI coordinates cortical patterning, neurogenesis, and laminar fate and modulates MAPK/ERK, AKT, and beta-catenin signaling. *Cereb. Cortex* **18**, 2117-2131.

Ge, W., He, F., Kim, K. J., Blanchi, B., Coskun, V., Nguyen, L., Wu, X., Zhao, J., Heng, J. I., Martinowich, K. et al. (2006). Coupling of cell migration with neurogenesis by proneural bHLH factors. *Proc. Natl. Acad. Sci. USA* **103**, 1319-1324.

Goebbels, S., Bormuth, I., Bode, U., Hermanson, O., Schwab, M. H. and Nave, K. A. (2006). Genetic targeting of principal neurons in neocortex and hippocampus of NEX-Cre mice. *Genesis* **44**, 611-621.

Hand, R., Bortone, D., Mattar, P., Nguyen, L., Heng, J. I., Guerrier, S., Boutt, E., Peters, E., Barnes, A. P., Parras, C. et al. (2005). Phosphorylation of Neurogenin2 specifies the migration properties and the dendritic morphology of pyramidal neurons in the neocortex. *Neuron* **48**, 45-62.

Hatanaka, Y. and Murakami, F. (2002). In vitro analysis of the origin, migratory behavior, and maturation of cortical pyramidal cells. *J. Comp. Neurol.* **454**, 1-14.

Heng, J. I., Nguyen, L., Castro, D. S., Zimmer, C., Wildner, H., Armant, O., Skowronska-Krawczyk, D., Bedogni, F., Matter, J. M., Hevner, R. et al. (2008). Neurogenin 2 controls cortical neuron migration through regulation of Rnd2. *Nature* **455**, 114-118.

Hevner, R. F., Shi, L., Justice, N., Hsueh, Y., Sheng, M., Smiga, S., Bulfone, A., Goffinet, A. M., Campagnoni, A. T. and Rubenstein, J. L. (2001). Tbr1 regulates differentiation of the preplate and layer 6. *Neuron* **29**, 353-366.

Hunter-Schaedle, K. E. (1997). Radial glial cell development and transformation are disturbed in reeler forebrain. *J. Neurobiol.* **33**, 459-472.

Kakimoto, T., Katoh, H. and Negishi, M. (2004). Identification of splicing variants of Rapostlin, a novel RND2 effector that interacts with neural Wiskott-Aldrich syndrome protein and induces neurite branching. *J. Biol. Chem.* **279**, 14104-14110.

Koizumi, H., Tanaka, T. and Gleeson, J. G. (2006). Doublecortin-like kinase functions with doublecortin to mediate fiber tract decussation and neuronal migration. *Neuron* **49**, 55-66.

Kowalczyk, T., Pontious, A., Englund, C., Daza, R. A., Bedogni, F., Hodge, R., Attardo, A., Bell, C., Huttner, W. B. and Hevner, R. F. (2009). Intermediate neuronal progenitors (basal progenitors) produce pyramidal-projection neurons for all layers of cerebral cortex. *Cereb. Cortex* **19**, 2439-2450.

Kuo, M. H. and Allis, C. D. (1999). In vivo cross-linking and immunoprecipitation for studying dynamic Protein:DNA associations in a chromatin environment. *Methods* **19**, 425-433.

Liu, Q., Dwyer, N. D. and O'Leary, D. D. (2000). Differential expression of COUP-TFI, CHL1, and two novel genes in developing neocortex identified by differential display PCR. *J. Neurosci.* **20**, 7682-7690.

Loots, G. and Ovcharenko, I. (2007). ECRbase: database of evolutionary conserved regions, promoters, and transcription factor binding sites in vertebrate genomes. *Bioinformatics* **23**, 122-124.

LoTurco, J. J. and Bai, J. (2006). The multipolar stage and disruptions in neuronal migration. *Trends Neurosci.* **29**, 407-413.

Marchetti, G., Escuin, S., van der Flier, A., De Arcangelis, A., Hynes, R. O. and Georges-Labouesse, E. (2010). Integrin alpha5beta1 is necessary for regulation of radial migration of cortical neurons during mouse brain development. *Eur. J. Neurosci.* **31**, 399-409.

Mitchell, B. D. and Macklis, J. D. (2005). Large-scale maintenance of dual projections by callosal and frontal cortical projection neurons in adult mice. *J. Comp. Neurol.* **482**, 17-32.

Miyata, T., Kawaguchi, A., Saito, K., Kawano, M., Muto, T. and Ogawa, M. (2004). Asymmetric production of surface-dividing and non-surface-dividing cortical progenitor cells. *Development* **131**, 3133-3145.

Molnar, Z., Metin, C., Stoykova, A., Tarabykin, V., Price, D. J., Francis, F., Meyer, G., Dehay, C. and Kennedy, H. (2006). Comparative aspects of cerebral cortical development. *Eur. J. Neurosci.* **23**, 921-934.

Molyneaux, B. J., Arlotta, P., Fame, R. M., MacDonald, J. L., MacQuarrie, K. L. and Macklis, J. D. (2009). Novel subtype-specific genes identify distinct subpopulations of callosal projection neurons. *J. Neurosci.* **29**, 12343-12354.

Montemayor, C., Montemayor, O. A., Ridgeway, A., Lin, F., Wheeler, D. A., Pletcher, S. D. and Pereira, F. A. (2010). Genome-wide analysis of binding sites and direct target genes of the orphan nuclear receptor NR2F1/COUP-TFI. *PLoS ONE* **5**, e8910.

Nadarajah, B., Brunstrom, J. E., Grutzendler, J., Wong, R. O. and Pearlman, A. L. (2001). Two modes of radial migration in early development of the cerebral cortex. *Nat. Neurosci.* **4**, 143-150.

Nadarajah, B., Alifragis, P., Wong, R. O. and Parnavelas, J. G. (2002). Ventricle-directed migration in the developing cerebral cortex. *Nat. Neurosci.* **5**, 218-224.

Nakamura, K., Yamashita, Y., Tamamaki, N., Katoh, H., Kaneko, T. and Negishi, M. (2006). In vivo function of Rnd2 in the development of neocortical pyramidal neurons. *Neurosci. Res.* **54**, 149-153.

Nguyen, L., Besson, A., Heng, J. I., Schuurmans, C., Teboul, L., Parras, C., Philpott, A., Roberts, J. M. and Guillemot, F. (2006). p27kip1 independently promotes neuronal differentiation and migration in the cerebral cortex. *Genes Dev.* **20**, 1511-1524.

Nieto, M., Monuki, E. S., Tang, H., Imitola, J., Haubst, N., Khoury, S. J., Cunningham, J., Gotz, M. and Walsh, C. A. (2004). Expression of Cux-1 and Cux-2 in the subventricular zone and upper layers II-IV of the cerebral cortex. *J. Comp. Neurol.* **479**, 168-180.

Nishihara, E., O'Malley, B. W. and Xu, J. (2004). Nuclear receptor coregulators are new players in nervous system development and function. *Mol. Neurobiol.* **30**, 307-325.

Niu, S., Renfro, A., Quattrocchi, C. C., Sheldon, M. and D'Arcangelo, G. (2004). Reelin promotes hippocampal dendrite development through the VLDLR/ApoER2-Dab1 pathway. *Neuron* **41**, 71-84.

Noctor, S. C., Martinez-Cerdeno, V., Ivic, L. and Kriegstein, A. R. (2004). Cortical neurons arise in symmetric and asymmetric division zones and migrate through specific phases. *Nat. Neurosci.* **7**, 136-144.

Norris, C. R. and Kalil, K. (1991). Guidance of callosal axons by radial glia in the developing cerebral cortex. *J. Neurosci.* **11**, 3481-3492.

Northcutt, R. G. and Kaas, J. H. (1995). The emergence and evolution of mammalian neocortex. *Trends Neurosci.* **18**, 373-379.

Ohshima, T., Hirasawa, M., Tabata, H., Mutoh, T., Adachi, T., Suzuki, H., Saruta, K., Iwasato, T., Itohara, S., Hashimoto, M. et al. (2007). Cdk5 is required for multipolar-to-bipolar transition during radial neuronal migration and proper dendrite development of pyramidal neurons in the cerebral cortex. *Development* **134**, 2273-2282.

O'Leary, D. D., Chou, S. J. and Sahara, S. (2007). Area patterning of the mammalian cortex. *Neuron* **56**, 252-269.

Olson, E. C., Kim, S. and Walsh, C. A. (2006). Impaired neuronal positioning and dendritogenesis in the neocortex after cell-autonomous Dab1 suppression. *J. Neurosci.* **26**, 1767-1775.

Pacary, E., Heng, J., Azzarelli, R., Riou, P., Castro, D., Lebel-Potter, M., Parras, C., Bell, D. M., Ridley, A. J., Parsons, M. et al. (2011). Proneural transcription factors regulate different steps of cortical neuron migration through Rnd-mediated inhibition of RhoA signaling. *Neuron* **69**, 1069-1084.

Quandt, K., Frech, K., Karas, H., Wingender, E. and Werner, T. (1995). MatInd and MatInspector: new fast and versatile tools for detection of consensus matches in nucleotide sequence data. *Nucleic Acids Res.* **23**, 4878-4884.

Rakic, P. (1978). Neuronal migration and contact guidance in the primate telencephalon. *Postgrad. Med. J.* **54**, 25-40.

Ramos, R. L., Tam, D. M. and Brumberg, J. C. (2008). Physiology and morphology of callosal projection neurons in mouse. *Neuroscience* **153**, 654-663.

Richards, L. J., Plachez, C. and Ren, T. (2004). Mechanisms regulating the development of the corpus callosum and its agenesis in mouse and human. *Clin. Genet.* **66**, 276-289.

Sanada, K., Gupta, A. and Tsai, L. H. (2004). Disabled-1-regulated adhesion of migrating neurons to radial glial fiber contributes to neuronal positioning during early corticogenesis. *Neuron* **42**, 197-211.

Sasaki, S., Tabata, H., Tachikawa, K. and Nakajima, K. (2008). The cortical subventricular zone-specific molecule Svet1 is part of the nuclear RNA coded by the putative netrin receptor gene Unc5d and is expressed in multipolar migrating cells. *Mol. Cell. Neurosci.* **38**, 474-483.

Seibt, J., Schuurmans, C., Gradwhol, G., Dehay, C., Vanderhaeghen, P., Guillemot, F. and Polleux, F. (2003). Neurogenin2 specifies the connectivity of thalamic neurons by controlling axon responsiveness to intermediate target cues. *Neuron* **39**, 439-452.

Sessa, A., Mao, C. A., Hadjantonakis, A. K., Klein, W. H. and Broccoli, V. (2008). Tbr2 directs conversion of radial glia into basal precursors and guides neuronal amplification by indirect neurogenesis in the developing neocortex. *Neuron* **60**, 56-69.

Shimogori, T. and Grove, E. A. (2005). Fibroblast growth factor 8 regulates neocortical guidance of area-specific thalamic innervation. *J. Neurosci.* **25**, 6550-6560.

Super, H. and Uylings, H. B. (2001). The early differentiation of the neocortex: a hypothesis on neocortical evolution. *Cereb. Cortex* **11**, 1101-1109.

Tabata, H. and Nakajima, K. (2003). Multipolar migration: the third mode of radial neuronal migration in the developing cerebral cortex. *J. Neurosci.* **23**, 9996-10001.

Takeuchi, A. and O'Leary, D. D. (2006). Radial migration of superficial layer cortical neurons controlled by novel Ig cell adhesion molecule MDGA1. *J. Neurosci.* **26**, 4460-4464.

Tanaka, H., Katoh, H. and Negishi, M. (2006). Pragmin, a novel effector of Rnd2 GTPase, stimulates RhoA activity. *J. Biol. Chem.* **281**, 10355-10364.

Tarabykin, V., Stoykova, A., Usman, N. and Gruss, P. (2001). Cortical upper layer neurons derive from the subventricular zone as indicated by Svet1 gene expression. *Development* **128**, 1983-1993.

Tomassy, G. S., De Leonibus, E., Jabaudon, D., Lodato, S., Alfano, C., Mele, A., Macklis, J. D. and Studer, M. (2010). Area-specific temporal control of corticospinal motor neuron differentiation by COUP-TFI. *Proc. Natl. Acad. Sci. USA* **107**, 3576-3581.

Tripodi, M., Filosa, A., Armentano, M. and Studer, M. (2004). The COUP-TF nuclear receptors regulate cell migration in the mammalian basal forebrain. *Development* **131**, 6119-6129.

Uesugi, K., Oinuma, I., Katoh, H. and Negishi, M. (2009). Different requirement for Rnd GTPases of R-Ras GAP activity of Plexin-C1 and Plexin-D1. *J. Biol. Chem.* **284**, 6743-6751.

Wang, C. L., Zhang, L., Zhou, Y., Zhou, J., Yang, X. J., Duan, S. M., Xiong, Z. Q. and Ding, Y. Q. (2007). Activity-dependent development of callosal projections in the somatosensory cortex. *J. Neurosci.* **27**, 11334-11342.

Zhang, L. J., Liu, X., Gafken, P. R., Kioussi, C. and Leid, M. (2009). A chicken ovalbumin upstream promoter transcription factor I (COUP-TFI) complex represses expression of the gene encoding tumor necrosis factor alpha-induced protein 8 (TNFAIP8). *J. Biol. Chem.* **284**, 6156-6168.

Zhou, C., Tsai, S. Y. and Tsai, M. J. (2001). COUP-TFI: an intrinsic factor for early regionalization of the neocortex. *Genes Dev.* **15**, 2054-2059.

Zimmer, C., Tiveron, M. C., Bodmer, R. and Cremer, H. (2004). Dynamics of Cux2 expression suggests that an early pool of SVZ precursors is fated to become upper cortical layer neurons. *Cereb. Cortex* **14**, 1408-1420.